Journal of Hydrology 617 (2023) 129142

Contents lists available at ScienceDirect

Journal of Hydrology

journal homepage: www.elsevier.com/locate/jhydrol

Research papers

Differences in watershed evaporation indicated by hydrogen and oxygen single and dual isotopes: Evidence from controlled simulation tests under different land uses

Yundi Hu [a,b,*], Hongdai Fan [a,b], Min Zhao [c,d], Deyong Hu [e], Qian Bao [f], Cheng Zeng [c,d], Dong Li [c], Yi Zhang [g,c], Fan Xia [c], Xianli Cai [c,d], Jia Chen [c,d], Zhongfa Zhou [a,b,*]

[a] School of Geography and Environmental Science, Guizhou Normal University, Guiyang 550025, China
[b] State Key Laboratory Incubation Base for Karst Mountain Ecology Environment of Guizhou Province, Guiyang 550025, China
[c] State Key Laboratory of Environmental Geochemistry, Institute of Geochemistry, CAS, Guiyang 550081, China
[d] Puding Karst Ecosystem Research Station, Chinese Ecosystem Research Network, Chinese Academy of Sciences, Puding 562100, China
[e] No.105 Geological Team, Guizhou Bureau of Geology and Mineral Exploration and Development, Guiyang 550018, China
[f] Key Laboratory of Land Resources Evaluation and Monitoring in Southwest China of Ministry of Education, Sichuan Normal University, Chengdu 610066, China
[g] School of Resources and Environmental Engineering, Guizhou Institute of Technology, Guiyang 550025, China

ARTICLE INFO

Keywords:
Watershed evaporation
Hydrogen and oxygen isotopes
Dual isotopes
D-excess
Lc-excess
Land use

ABSTRACT

Partitioning watershed evapotranspiration into evaporation and transpiration is essential for studying the water–carbon cycle, and the key step in this partitioning is to calculate watershed evaporation based on isotopic indexes. The $\delta^{18}O$ and $\delta^{2}H$ single isotopes and d-excess or lc-excess dual isotopes derived from $\delta^{18}O$ and $\delta^{2}H$ are widely used for this purpose. Although $\delta^{18}O$, $\delta^{2}H$, and d-excess have different characteristics, few studies have assessed how these differences influence the usefulness of these isotopes as indicators of watershed evaporation. Here, we simulated five watersheds with different land uses and degrees of evaporation in a region of Southwest China with a subtropical monsoon climate. We then investigated differences in the ability of the isotopic indexes to indicate watershed evaporation over two hydrological years. We found that d-excess and lc-excess dual isotopes were better indicators of watershed evaporation than $\delta^{18}O$ and $\delta^{2}H$ single isotopes. This is because the $\delta^{18}O$ and $\delta^{2}H$ in precipitation are easily influenced by rainout during the rainy season, when groundwater is primarily recharged. They are more variable than d-excess and lc-excess, which leads to $\delta^{18}O$ and $\delta^{2}H$ in groundwater being more sensitive to changes in the isotopic signal input in precipitation. This probably interferes with, or even masks watershed evaporation signals carried by $\delta^{18}O$ and $\delta^{2}H$. The annual mean isotopic compositions were more depleted in groundwaters ($\delta^{18}O = -8.7$ ‰ to -8.5 ‰, $\delta^{2}H = -61.9$ ‰ to -58.7 ‰) than in precipitation ($\delta^{18}O = -8.3$ ‰, $\delta^{2}H = -54.3$ ‰) from November 2015 to October 2016; these compositions fail to support the isotopic enrichment of groundwater compared with that of precipitation. Evaporation rates over two years derived from d-excess dual isotopes agreed well with those from the water balance in bare-rock and bare-soil lands, which had no data from plants available for verification. Compared with hydrogen and oxygen single isotopes, their dual isotopes reflected watershed evaporation more accurately, especially in Asian monsoon regions.

1. Introduction

Terrestrial evapotranspiration (ET) is a combination of physical evaporation (E) from open water and soil and transpiration (T) from plants. Because of plant water-use efficiency, water (transpiration) and the carbon cycle are linked by CO_2 uptake and water vapor release during photosynthesis (Lee and Veizer, 2003; Beer et al., 2007). Water and carbon flux influence the global climate (Ferguson and Veizer, 2007; Berg and Sheffield, 2019), and watershed-based evaluation allows the estimation of water and carbon flux at regional to continental scales. Therefore, separating T from ET flux at the watershed scale is important when investigating the global water–carbon cycle.

* Corresponding authors at: School of Geography and Environmental Science, Guizhou Normal University, Guiyang 550025, China.
E-mail addresses: hydhydro@163.com (Y. Hu), fa6897@163.com (Z. Zhou).

https://doi.org/10.1016/j.jhydrol.2023.129142
Received 12 July 2022; Received in revised form 28 September 2022; Accepted 16 January 2023
Available online 20 January 2023

Partitioning ET is accurate at the point scale, but not so much at the watershed scale, and attempts to do so have been scant (Sulman et al., 2016). Strategies that have been applied to ET partitioning, include field measurement, land surface models, and aqueous isotope analysis. Field measurement is valid primarily for quantifying items such as sap flow, lysimetry, and eddy covariance at the plot scale (Van der Tol et al., 2003; Mitchell et al., 2009; Kool et al., 2014; Ren et al., 2022). Although field measurements can be reasonably accurate, extrapolating them to E and T at the watershed scale might hampered by the heterogeneity of watersheds. Land surface models can yield large-scale E and T estimates, but downscaling or upscaling problems may arise when they are applied to a watershed because some meteorological and vegetation parameters of models, are typically based on remote sensing or plot measurement (Sutanto et al., 2014). Isotope-based methods can be used to partition ET at plot and watershed scales, because E and T fractionate aqueous isotopes differently (Wershaw et al., 1966; Ehleringer and Dawson, 1992). However, ET partitioning at the plot scale is costly and labor-intensive, and often requires measurements of diurnal leaf water (Wang and Yakir, 2000; Yepez et al., 2003; Williams et al., 2004; Han et al., 2022). Watershed-based ET partitioning can be achieved based on differences in isotopic composition between outflowing water at a watershed outlet and its precipitation input (Ferguson et al., 2007; Jasechko et al., 2013; Good et al., 2015; Gibson et al., 2021). This is because watershed E can be estimated from these differences, then watershed T can be indirectly estimated by subtracting E from ET obtained from the watershed water balance. This method is usually applied on the timescale of hydrological year, given the hydrologic residence times in most watersheds (Jasechko et al., 2013) and changes in water storage are approximately zero on that timescale, which simplifies the watershed water balance (Lee and Veizer, 2003; Zhao et al., 2018).

The T/ET estimated using different methods is typically discrepant. For example, T/ET estimates based on isotopic measurements are typically higher than estimates obtained by other methods but tend to be closer overall to those obtained from field measurements than from land surface models (Schlesinger and Jasechko, 2014; Sutanto et al., 2014; Xiao et al., 2018). Therefore, isotope-based methods play an important role in ET partitioning. The key step in watershed-based partitioning is accurately estimating watershed E based on isotopic indexes.

Recent studies have shown that watershed E can be estimated using two types of aqueous isotopic indexes. The first type is a hydrogen or oxygen single-isotope index (δ^2H or $\delta^{18}O$). The second type is a hydrogen and oxygen dual-isotope index, such as deuterium excess (d-excess) and line-conditioned excess (lc-excess) (Dansgaard, 1964; Landwehr and Coplen, 2004). Both types of isotopic indexes can indicate watershed E (Landwehr and Coplen, 2004; Evaristo et al., 2015; Gonfiantini et al., 2018; Hu et al., 2018; Lyu et al., 2021). When groundwater or soil water is recharged by precipitation in a watershed with evaporation that occurs during infiltration, the δ^2H and $\delta^{18}O$ of the precipitation will plot along the evaporation line (Clark and Fritz, 1997), e.g., from A to B or A′ to B′ (Fig. 1). This will be accompanied by enriched δ^2H and $\delta^{18}O$, decreased d-excess and lc-excess, and increased deviation from the meteoric water line, which is the distance from groundwater to this line on the vertical axis (Fig. 1). Watershed E can then be estimated as the differences in isotopic composition between outflowing water and its precipitation input, with larger differences indicating more E. However, δ^2H and $\delta^{18}O$ are more widely used than d-excess and lc-excess (Gibson et al., 1993; Telmer and Veizer, 2000; Horita et al., 2008; Gibson et al., 2021). The characteristics of δ^2H, $\delta^{18}O$, and d-excess differ in precipitation (Huang and Pang, 2012; Hu et al., 2018). For example, when δ^2H and $\delta^{18}O$ vary in different precipitation events, d-excess could remain unchanged (e.g., A and A′) (Fig. 1). The isotopic indexes in precipitation, such as the main isotopic signal input in many watersheds, are essential to estimating watershed E. However, whether the characteristics of these isotopic indexes affect the accuracy of watershed E estimation remains unclear.

Thus, given the scarcity of true E values in natural watersheds, we simulated five watersheds with different land uses at the Shawan Test Site in Guizhou, Southwest China. The study has the following specific objectives: (1) define the integrated E of groundwater under different land uses in $\delta^{18}O$-δ^2H plots; (2) determine variations of $\delta^{18}O$, δ^2H, d-excess, and lc-excess in precipitation input and groundwater output; (3) based on these variations, evaluate the roles that $\delta^{18}O$, δ^2H, d-excess, and lc-excess play in determining watershed E; and (4) determine whether E results derived from the isotope-based method and from water balance differ between two simulated watersheds without plants. The present findings will be essential for selecting appropriate isotopic indexes to estimate watershed E.

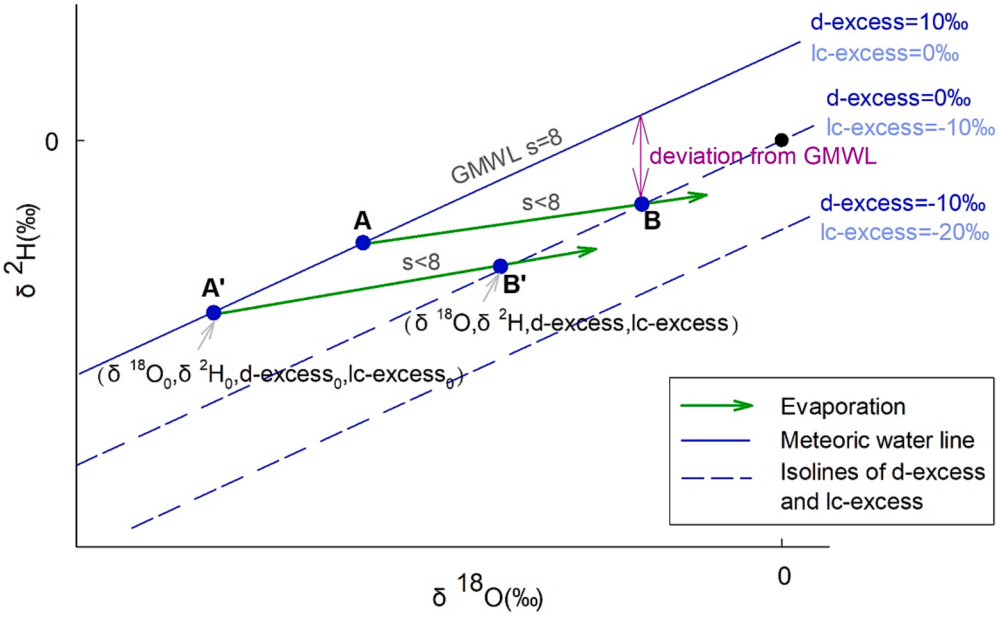

Fig. 1. Variations in $\delta^{18}O$, δ^2H, d-excess, and lc-excess during evaporation of precipitation. Evaporation proceeding from A to B or A′ to B′ is accompanied by enriched $\delta^{18}O$ and δ^2H, decreased d-excess and lc-excess, and increased deviation from the meteoric water line. Slope (s) of global meteoric water line (GMWL) (s = 8) is taken as a reference in δ^2H–$\delta^{18}O$ plots ($s = (\delta^2H-\delta^2H_0)/(\delta^{18}O-\delta^{18}O_0) = (\alpha^2H-1)/(\alpha^{18}O-1)$ (Clark and Fritz, 1997)).

2. Study site

The Shawan Test Site is located in the Puding Comprehensive Karst Research and Experimental Station (26°14′–26°15′N, 105°42′–105°43′E, 1200 m), Guizhou Province, Southwest China (Fig. 2a and b). The study area is characterized by a typical, humid, subtropical, monsoonal climate, with an annual mean air temperature of 15.2 °C and annual mean precipitation of 1,341 mm, of which >80 % occurs during the rainy season (May–October) (Zhao et al., 2010; Yang et al., 2012). These values are based on 30 years of data (1981–2010) from the China Meteorological Data Network. A meteorological station in Puding Station (Fig. 2c), installed within 100 m of Shawan Test Site, collected daily precipitation, air temperature, and relative humidity data.

Five adjoining concrete tanks at the site were constructed to simulate watersheds under land comprising bare-rock, bare-soil, cultivation, grass, and shrub growth (Fig. 2b). Each tank was 20 m long, 5 m wide, 3 m deep, coated with epoxy resin, and covered with a high-density polyethylene (HDPE) film to create an impervious boundary. These tanks contained 2.5 m of dolomitic limestone gravel from the local Guanling Formation (Middle Triassic) to serve as a granular aquifer with a porosity of ~0.5 (Zhu et al., 2015). The surface of the bare-rock tank comprised gravel without soil or vegetation. The other four tanks were covered with 0.5 m of clay-rich residual soil on top of the gravel surface, and the bare-soil tank contained only soil without vegetation. Corn, alfalfa, and Roxburgh roses were planted in the remaining three tanks to simulate land that was regularly cultivated, had perennial grass, and shrub growth, respectively. Corn was present only during the growing season between April to August, whereas alfalfa and Roxburgh roses were sown in January 2014 and left undisturbed. Degree of vegetation development comprised grassland > shrub land > cultivated land. More details can be found in the studies by Zeng et al. (2017), Bao et al. (2020), and Hu et al. (2020). A lateral drainage hole in each tank simulated a natural karst spring, and an adjoining piezometer measured groundwater levels (Fig. 2d). These tanks functioned as natural watersheds that are recharged by natural rainfall that infiltrates them through vegetation, soil, and aquifers (coarse dolomitic limestone gravel) and discharges at simulated springs; therefore, we termed them simulated watersheds. Thus, the land use of the five simulated watersheds differed under identical climatic input and hydrogeological conditions.

3. Methods

3.1. Sampling and analysis

A total of 190 rainfall events (~92 % of the precipitation events between November 2015 to October 2017) were sampled using standard gauges based on IAEA/GNIP guidelines for precipitation sampling. After each rainfall event, rainfall samples were immediately passed through 0.45-μm Millipore filters into 20-mL HDPE bottles to prevent evaporation. Samples were collected from simulated springs at 10-day intervals to obtain high-resolution groundwater isotopic data. Groundwater discharges and water levels were also measured. Groundwater samples were passed through Millipore filters and stored at ~4 °C in HDPE bottles sealed with Parafilm. The meteorological data were obtained from the meteorological station at the Puding Station. The $\delta^{18}O$ and $\delta^{2}H$

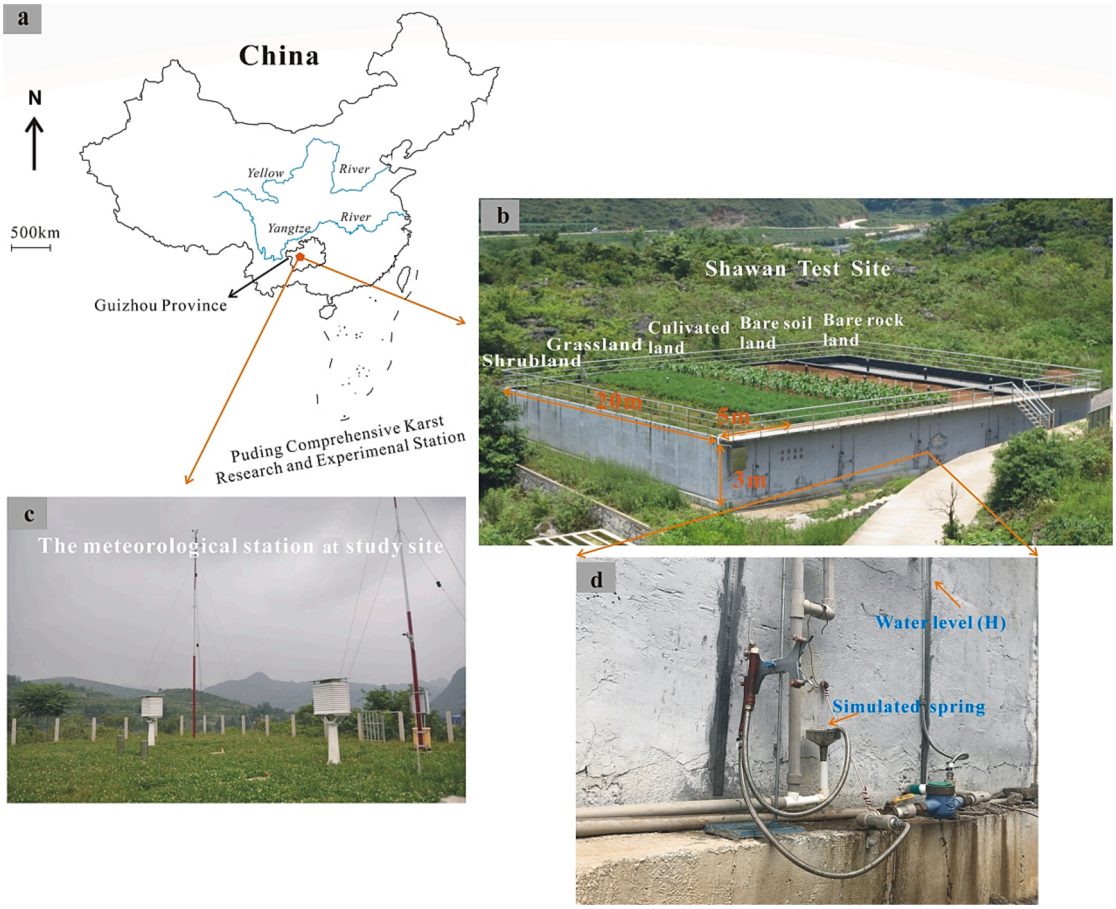

Fig. 2. (a) Location of Puding Comprehensive Karst Research and Experimental Station in Guizhou Province, Southwest China. (b) Five concrete tanks simulate watersheds with bare-rock (coarse gravel), bare-soil, cultivated (corn), grassland (alfalfa), and shrub (Roxburgh roses) at Shawan Test Site. (c) Meteorological station at Puding Station, within 100 m of Shawan Test Site. (d) Simulated spring and piezometer for measuring levels of groundwater in tanks.

values of the precipitation and groundwater samples were assessed at the State Key Laboratory of Environmental Geochemistry, Institute of Geochemistry, Chinese Academy of Sciences, using a Los Gatos Research DLT-100 liquid isotope water analyzer (Lis et al., 2008). All samples were equilibrated for at least 2 h at room temperature (25 °C) before assay. The isotopic compositions (δ^2H, δ^{18}O) of the standards (Los Gatos Research Inc) was (−123.6 ‰, −16.1 ‰) for LGR2A, (−96.4 ‰, −13.1 ‰) for LGR3A, (−51.0 ‰, −7.7 ‰) for LGR4A, and (−9.5 ‰, −2.8 ‰) for LGR5A. These standards encompassed the isotopic range of the measured samples. The standard deviation (1σ) of the δ^{18}O and δ^2H measurements was ±0.1 ‰ and ±0.5 ‰, respectively. All values are shown *versus* Vienna Standard Mean Ocean Water.

3.2. Theoretical background

3.2.1. ET estimation using water balance

The ET of a watershed can be estimated using the water balance (Wisler and Brater, 1959) as follows:

$$ET = P - discharge - \Delta S \tag{1}$$

where ET is evapotranspiration, P is precipitation, and △S is the change in water storage. Due to a lack of surface runoff in the five simple watersheds, discharge was taken as groundwater discharge. Given that changes in soil water storage are near zero on the timescale of a hydrological year, △S represents changes in groundwater storage. Thus, discharge + △S is the amount of groundwater recharge from precipitation and the annual ratio of ET to precipitation can be determined using Eq. (2). Because vegetation did not develop in bare-rock and bare-soil lands, their ET values were only from E.

$$ET\% = (P - discharge - \Delta S)/P \tag{2}$$

3.2.2. Dual isotopes of d-excess and lc-excess

Based on the global meteoric water line (GMWL: $\delta^2H = 8\delta^{18}O + 10$) (Craig, 1961), Dansgaard (1964) defined the parameter of d-excess [Eq. (3)]. It can be deduced that the mean d-excess value of global precipitation was ~10 ‰. In comparison, Landwehr and Coplen (2004) proposed a new parameter, lc-excess [Eq. (4)], with respect to the local meteoric water line (LMWL: $\delta^2H = a\delta^{18}O + b$, where a and b are the slope and intercept of the LMWL, respectively). The lc-excess of precipitation plotted on the LMWL was ~0 ‰.

$$d - excess = \delta^2H - 8\delta^{18}O \tag{3}$$

$$lc - excess = \delta^2H - a\delta^{18}O - b \tag{4}$$

The d-excess and lc-excess that characterize co-variations in hydrogen and oxygen isotopes facilitated screening water samples with respect to meteoric conditions. For example, when E occurs in water samples and plots on the right side of GMWL and LMWL, they will be accompanied by d-excess < 10 ‰ and lc-excess < 0 ‰.

3.2.3. Estimation of E using d-excess dual isotopes

An evaporating water body evolves as described by the Rayleigh process (Clark and Fritz, 1997). E in a watershed water cycle is assumed to follow Rayleigh fractionation, as given in Eq. (5), where R represents either the $^{18}O/^{16}O$ or the $^2H/^1H$ ratio. We use δ instead of R for convenience, which expresses the Rayleigh fractionation [Eq. (6)]. Thereafter, the d-excess dual isotopes can be transformed into Eq. (7) based on Eq. (6). Accordingly, d-excess and the residual fraction of groundwater (f) were built through Eq. (7), where 1 − f means the ratio of E to precipitation in a watershed (i.e., E = 1 − f).

$$R = R_0 f^{(\alpha-1)} \tag{5}$$

$$\delta = (\delta_0 + 1000) f^{(\alpha-1)} - 1000 \tag{6}$$

$$\begin{aligned} d - excess &= \delta^2H - 8\delta^{18}O \\ &= \left(\delta^2H_0 + 1000\right)f^{(\alpha 2H-1)} - 1000 - 8\left(\left(\delta^{18}O_0 + 1000\right)f^{(\alpha 18O-1)} - 1000\right) \\ &= \left(\delta^2H_0 + 1000\right)f^{(\alpha 2H-1)} - 8\left(\delta^{18}O_0 + 1000\right)f^{(\alpha 18O-1)} + 7000 \end{aligned} \tag{7}$$

In the above equation, α is the fractionation factor that includes the equilibrium and kinetic fractionation factors [$\alpha = 1/(\alpha^* + \triangle\varepsilon)$]. α^* is the equilibrium fractionation factor that is dependent on temperature in Kelvins (t) [Eqs. (8) and (9)] and $\triangle\varepsilon$ is a dynamic enrichment factor that is associated with humidity (h) [Eqs. (10) and (11)] (Gonfiantini, 1986; Clark and Fritz, 1997; Majoube, 1971). $\delta^{18}O_0$ and δ^2H_0 are the initial isotopic compositions of groundwater, and d-excess is the isotopic compositions of groundwater in the watershed outlet.

$$1000\ln\alpha^{*2}H = 24.844\left(10^6/t^2\right) - 76.248\left(10^3/t\right) + 52.612 \tag{8}$$

$$1000\ln\alpha^{*18}O = 1.137\left(10^6/t^2\right) - 0.4156\left(10^3/t\right) - 2.0667 \tag{9}$$

$$\Delta\varepsilon^2H = 12.5(1-h)/1000 \tag{10}$$

$$\Delta\varepsilon^{18}O = 14.2(1-h)/1000 \tag{11}$$

The E is estimated on an annual timescale. Therefore, based on annual mean temperature, relative humidity, the initial isotopic compositions of groundwater inferred from the annual amount-weighted mean of the precipitation and annual mean isotopic composition of groundwater, the watershed E (E = 1 − f) can be calculated using Eq. (7).

Thereafter, the ratio of transpiration to precipitation (T) can be estimated by ET using the water balance and by E using the d-excess as:

$$T = ET - E \tag{12}$$

4. Results

4.1. Hydrological data

The groundwater discharges and water levels of the five land uses are shown in Fig. 3. In response to the input of precipitation in a subtropical monsoon climate, all variables were maxima during the rainy season and minima during the dry season. Furthermore, groundwater discharges and water levels differed according to land use.

Based on precipitation, groundwater levels, and discharge data, the proportion of groundwater recharged by precipitation during different seasons was estimated through the water balance (Table 1). The recharge results were 84.0 % for bare-rock land, 80.4 % for bare-soil land, 79.3 % for cultivated land, 70.9 % for grassland, and 86.5 % for shrub land during the rainy season from November 2015 to October 2016 and 88.9 % for bare-rock land, 94.8 % for bare-soil land, 94.3 % for cultivated land, 110.0 % for grassland, and 96 % for shrub land for the rainy season from November 2016 to October 2017. These results suggested that groundwater was primarily recharged by precipitation during the rainy season. Furthermore, the infiltration rate and ET in a hydrological year were calculated, as shown in Table 1.

4.2. Precipitation and groundwater in $\delta^{18}O - \delta^2H$ plots

We established the LMWL of the study area using rainfall samples collected from November 2015 to October 2017. The LMWL was $\delta^2H = 8.65\delta^{18}O + 18.00$ ($R^2 = 0.98$, $p < 0.0001$; Fig. 4a). The $\delta^{18}O$ and δ^2H of groundwater in the five watersheds lags behind precipitation. Based on lag times between groundwater and precipitation calculated by Hu et al. (2020), we shifted the $\delta^{18}O$ and δ^2H of groundwater back in time with respect to the precipitation input to obtain the groundwater isotopic data analyzed herein.

Fig. 4b1 and b2 shows that almost all groundwaters plotted to the right of the LMWL and displayed similar trends with it over the two-year

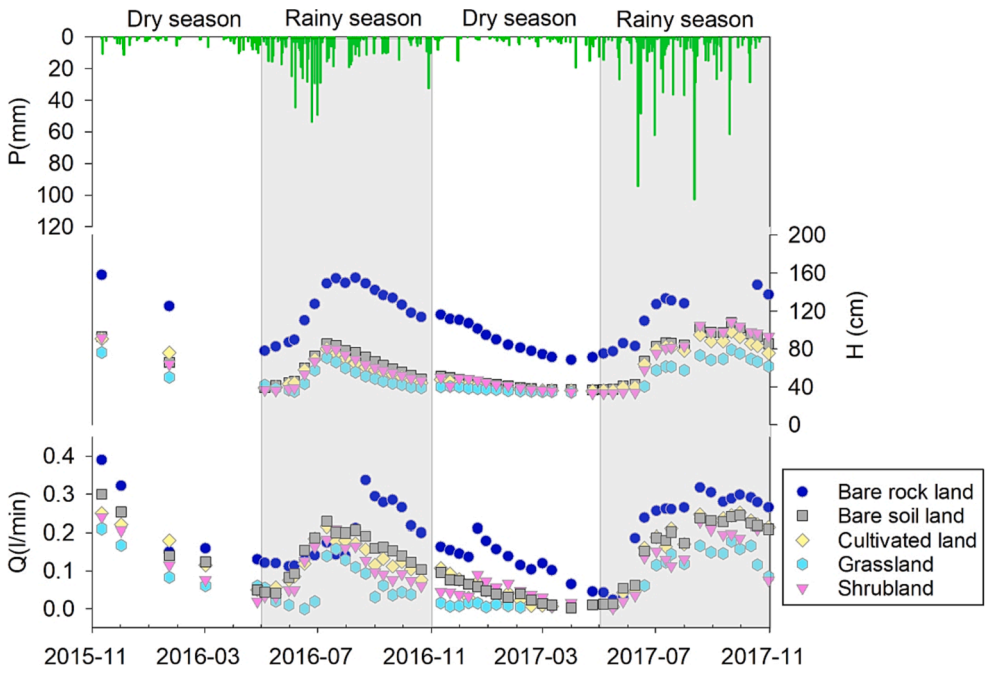

Fig. 3. Seasonal variations in precipitation (P), groundwater levels (H), and discharges (Q) at Shawan Test Site.

Table 1
Precipitation (P), water level change (△H), groundwater discharge, recharge, infiltration and evapotranspiration for the five simulated watersheds from November 2015 to October 2017.

Period	Water type	P(m)		△H (m)		Discharge (m)		Recharge[b] (%)		Infiltration rate[c] (%)	ET[d] (%)
		DS[a]	RS[a]	DS	RS	DS	RS	DS	RS		
2015/11–2016/10	Bare rock	0.181	0.804	−0.890	0.470	0.593	0.544	16.0	84.0	94.1	5.9 ± 3.3
	Bare soil			−0.620	0.200	0.433	0.405	19.6	80.4	63.8	36.2 ± 2.4
	Cultivated			−0.615	0.185	0.429	0.371	20.7	79.3	59.4	40.6 ± 2.6
	Grassland			−0.462	0.102	0.334	0.200	29.1	70.9	35.9	64.1 ± 1.0
	Shrubland			−0.550	0.130	0.332	0.300	13.5	86.5	42.8	57.2 ± 1.5
2016/11–2017/10	Bare rock	0.157	1.019	−0.448	0.621	0.344	0.650	11.1	88.9	98.1	1.9 ± 1.6
	Bare soil			−0.142	0.488	0.110	0.478	5.2	94.8	70.2	29.8 ± 1.1
	Cultivated			−0.121	0.395	0.099	0.442	5.7	94.3	60.6	39.4 ± 1.0
	Grassland			−0.112	0.331	0.017	0.267	−10.0	110.0	35.2	64.8 ± 0.6
	Shrubland			−0.165	0.594	0.110	0.346	4.0	96.0	58.9	41.1 ± 0.9

[a] DS: dry season (November–April); RS: rainy season (May–October).
[b] Recharge is the amount of groundwater supplied by precipitation. Recharge=△S + Discharge, where △S=△H*Porosity. The porosity value (0.5) is from Zhu et al. (2015). Recharge (%) in a given season is the recharge in that season divided by the recharge in the hydrological year.
[c] Infiltration rate is the ratio of recharge to precipitation, calculated as (△S + Discharge)/P.
[d] Ratio of evapotranspiration to precipitation, calculated using Eq. (2): ET%=(P- Discharge -△S)/P. Infiltration rate + ET = 1.

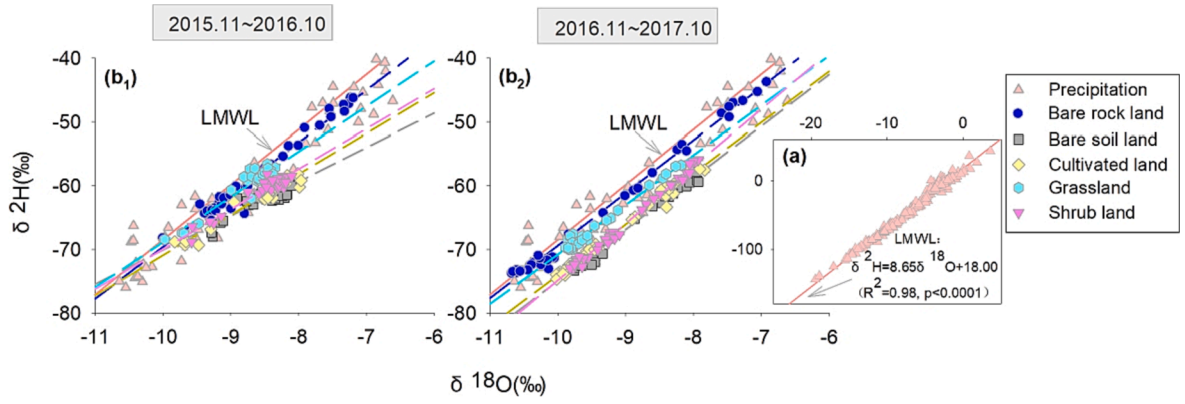

Fig. 4. Plots of $\delta^{18}O$–$\delta^{2}H$ in precipitation (a) and groundwater from November 2015 to October 2016 (b_1) and from November 2016 to October 2017 (b_2). Colored dashed lines represent best fit of groundwater under different land uses. Fitting details can be found in the text.

study period. From November 2015 to October 2016, the best fit for the groundwater data was $\delta^2H = 8.18\delta^{18}O + 12.31$ ($R^2 = 0.97$, $p < 0.0001$) for bare-rock land, $\delta^2H = 5.37\delta^{18}O$-16.37 ($R^2 = 0.77$, $p < 0.0001$) for bare-soil land, $\delta^2H = 6.37\delta^{18}O-7.15$ ($R^2 = 0.92$, $p < 0.0001$) for cultivated land, $\delta^2H = 7.10\delta^{18}O + 2.19$ ($R^2 = 0.88$, $p < 0.0001$) for grassland, and $\delta^2H = 6.29\delta^{18}O-7.00$ ($R^2 = 0.91$, $p < 0.0001$) for shrub land. From November 2016 to October 2017, these were $\delta^2H = 8.27\delta^{18}O + 13.36$ ($R^2 = 0.99$, $p < 0.0001$) for bare-rock land, $\delta^2H = 8.10\delta^{18}O + 6.05$ ($R^2 = 0.99$, $p < 0.0001$) for bare-soil land, $\delta^2H = 8.00\delta^{18}O + 5.95$ ($R^2 = 0.99$, $p < 0.0001$) for cultivated land, $\delta^2H = 7.79\delta^{18}O + 7.17$ ($R^2 = 0.97$, $p < 0.0001$) for grassland, and $\delta^2H = 8.95\delta^{18}O + 14.65$ ($R^2 = 0.99$, $p < 0.0001$) for shrub land.

4.3. Seasonal variations of $\delta^{18}O$, δ^2H, d-excess, and lc-excess in precipitation and groundwater

The $\delta^{18}O$, δ^2H, d-excess, and lc-excess values in precipitation exhibited notable seasonal variations, with $\delta^{18}O$ and δ^2H being depleted and enriched, respectively, and d-excess and lc-excess being low and high, respectively, during rainy season and dry season (Fig. 5). These variations were primarily attributable to different water vapor sources during the two seasons in a monsoon climate. Water vapor during the rainy season primarily originates from low-latitude, humid, and hot marine air masses, resulting in depleted $\delta^{18}O$ and δ^2H, and low d-excess values, whereas water vapor during the dry season primarily comes from cold and dry continental air masses, resulting in enriched $\delta^{18}O$ and δ^2H, and high d-excess values (Zhao et al., 2018; Zhou et al., 2019). Variations of lc-excess and d-excess were similar in precipitation. We calculated the annual amount-weighted averages of $\delta^{18}O$, δ^2H, d-excess, and lc-excess in precipitation based on rainfall data (Fig. 5, Table 2). Furthermore, rainfall during the rainy season accounted for 82 % and 87 % of the annual amount, respectively, between the first (November 2015–October 2016), and the second year (November 2016–October 2017) (Table 1). Therefore, given the dominance of precipitation during the rainy season, the mean value and standard deviation (STDEV) of $\delta^{18}O$, δ^2H, d-excess, and lc-excess of precipitation during the rainy season were also calculated (Table 2).

Fig. 6 shows seasonal variations of $\delta^{18}O$, δ^2H, d-excess, and lc-excess in groundwater of the five watersheds. The variations in $\delta^{18}O$ and δ^2H are clearly seasonal, being respectively depleted and enriched during the rainy and dry seasons. In comparison, d-excess and lc-excess did not vary seasonally and were relatively stable over the two years. The annual mean groundwater for the five land uses was calculated (Table 2; colored dashed line in Fig. 6). The analysis of variance (ANOVA) (Fig. 7) showed that the annual mean values of d-excess and lc-excess in groundwater significant differed ($p < 0.05$) among the five land uses during the study period, whereas those of $\delta^{18}O$ and δ^2H did not ($p > 0.05$). Overall, the d-excess and lc-excess of groundwater follow the

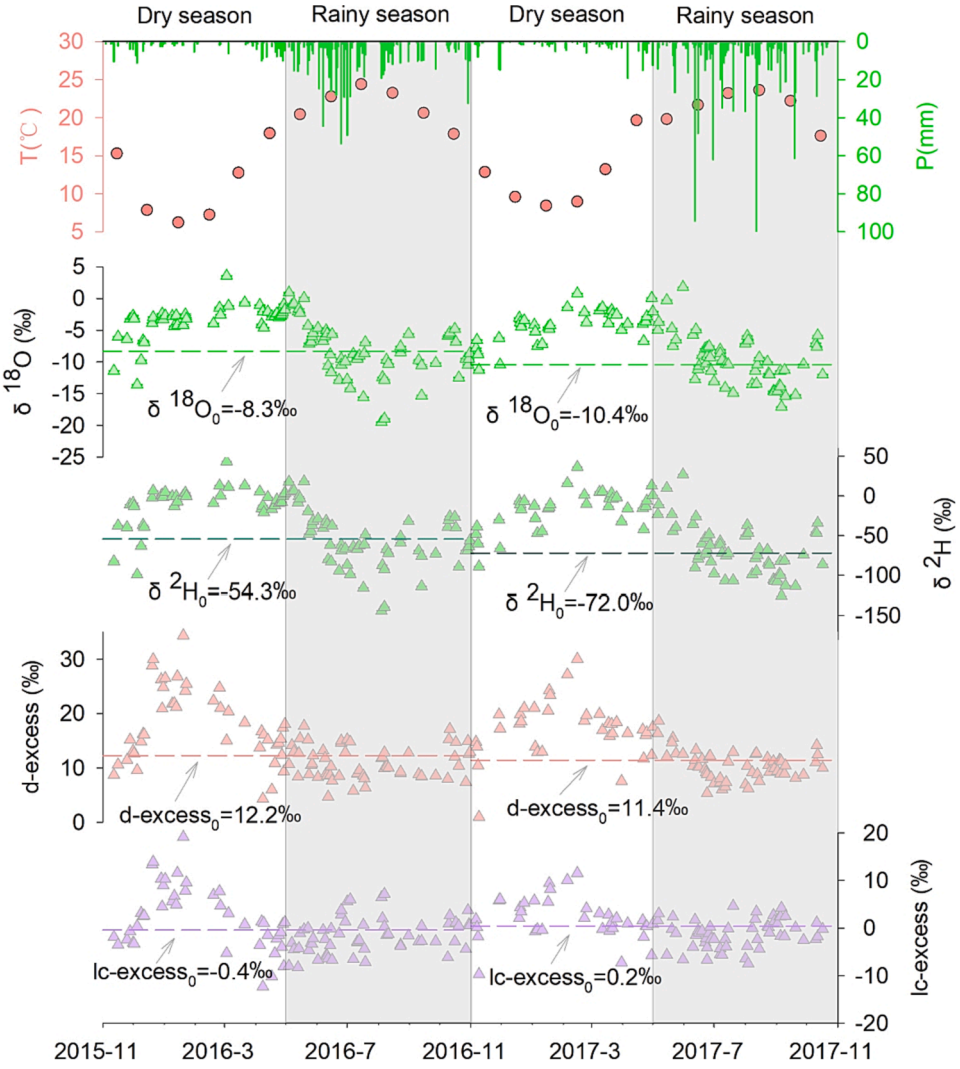

Fig. 5. Temporal variations in temperature (T), daily rainfall (P), and $\delta^{18}O$, δ^2H, d-excess, and lc-excess of precipitation. Dashed lines represent annual amount-weighted averages of precipitation.

Table 2
The annual mean values of $\delta^{18}O$, $\delta^{2}H$, d-excess and lc-excess for precipitation and groundwater in the simulated watersheds from November 2015 to October 2017.

Period	Water type	$\delta^{18}O$ (‰)		$\delta^{2}H$ (‰)		d-excess (‰)		lc-excess (‰)	
		Mean[a]	STDEV[b]	Mean[a]	STDEV[b]	Mean[a]	STDEV[b]	Mean[a]	STDEV[b]
2015/11–2016/10	Precipitation	−8.3	4.3	−54.3	37.5	12.2	6.0	−0.4	5.5
	Rainy season precipitation[c]	−8.2	4.3	−54.8	35.0	11.0	3.0	−1.7	3.7
	Bare rock	−8.7	0.8	−58.7	6.9	10.7	1.2	−1.7	1.2
	Bare soil	−8.5	0.3	−61.9	2.1	5.9	1.3	−6.6	1.5
	Cultivated	−8.6	0.5	−61.7	3.2	6.8	1.2	−5.7	1.5
	Grassland	−8.7	0.4	−59.5	3.1	10.0	1.1	−2.4	1.2
	Shrubland	−8.5	0.4	−60.6	2.6	7.5	1.0	−4.9	1.2
2016/11–2017/10	Precipitation	−10.4	4.4	−72.0	38.9	11.4	5.0	0.2	3.9
	Rainy season precipitation[c]	−9.7	3.9	−66.6	32.8	10.6	2.8	−1.1	3.0
	Bare rock	−9.3	1.3	−63.7	10.7	10.8	0.9	−1.1	1.0
	Bare soil	−9.0	0.7	−67.1	5.9	5.2	0.7	−7.0	0.8
	Cultivated	−9.3	0.7	−68.2	5.8	6.0	0.6	−6.0	0.8
	Grassland	−9.5	0.5	−66.7	4.1	9.1	0.7	−2.7	0.8
	Shrubland	−9.0	0.7	−65.6	5.8	6.2	0.8	−6.0	0.6

[a] The mean $\delta^{18}O$ and $\delta^{2}H$ of precipitation are expressed by annual amount-weighted values of $\delta^{18}O$ and $\delta^{2}H$, and other means are based on arithmetic averages.
[b] STDEV = standard deviation.
[c] Precipitation from May to October.

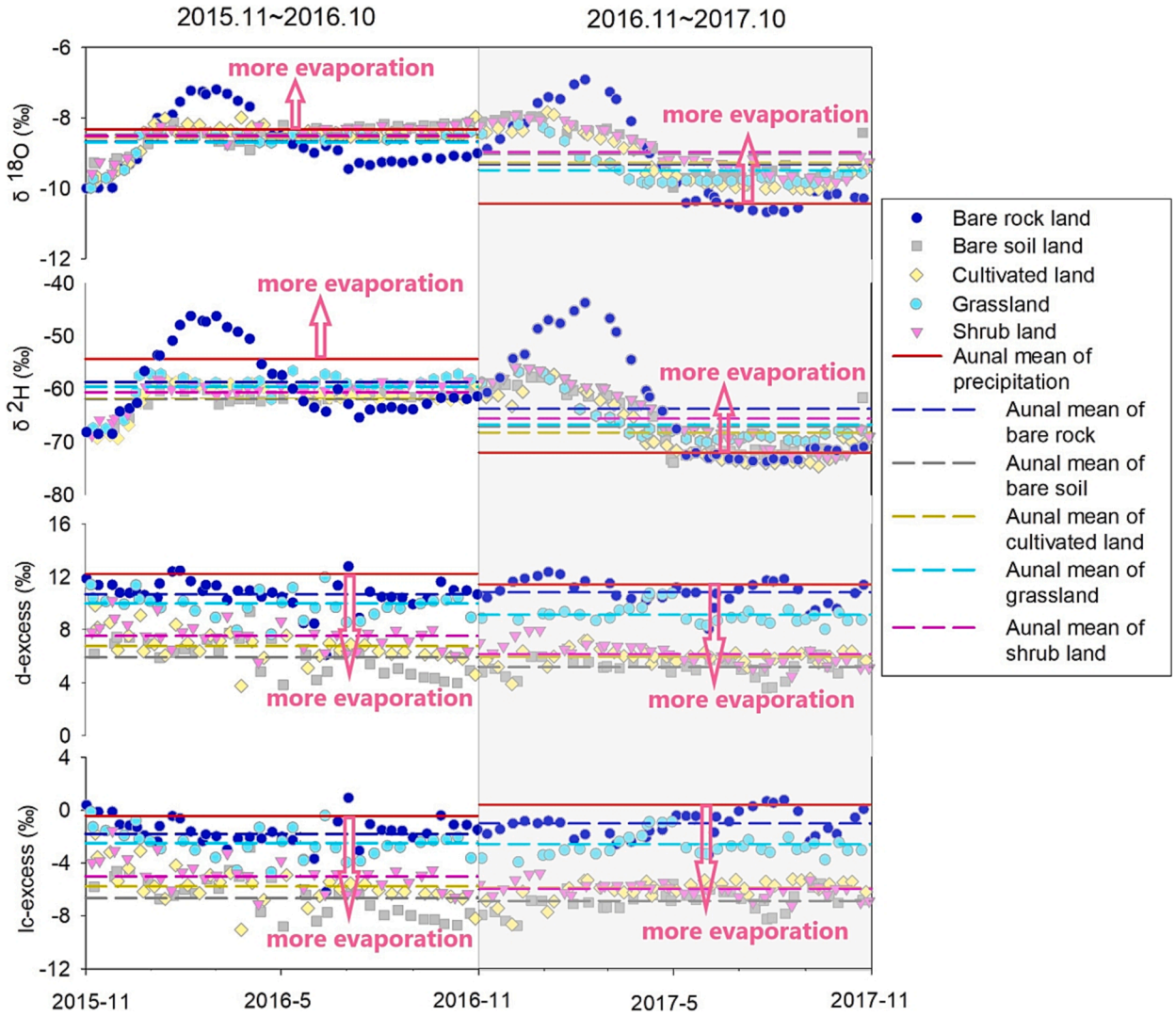

Fig. 6. Seasonal variations in $\delta^{18}O$, $\delta^{2}H$, d-excess, and lc-excess in groundwater from November 2015 to October 2017. Their annual mean values are represented by colored dashed lines indicating evaporation (i.e., more evaporation implies more $\delta^{18}O$ and $\delta^{2}H$ enrichment between groundwater and precipitation and lower d-excess and lc-excess values). Annual mean of precipitation represents annual amount-weighted average.

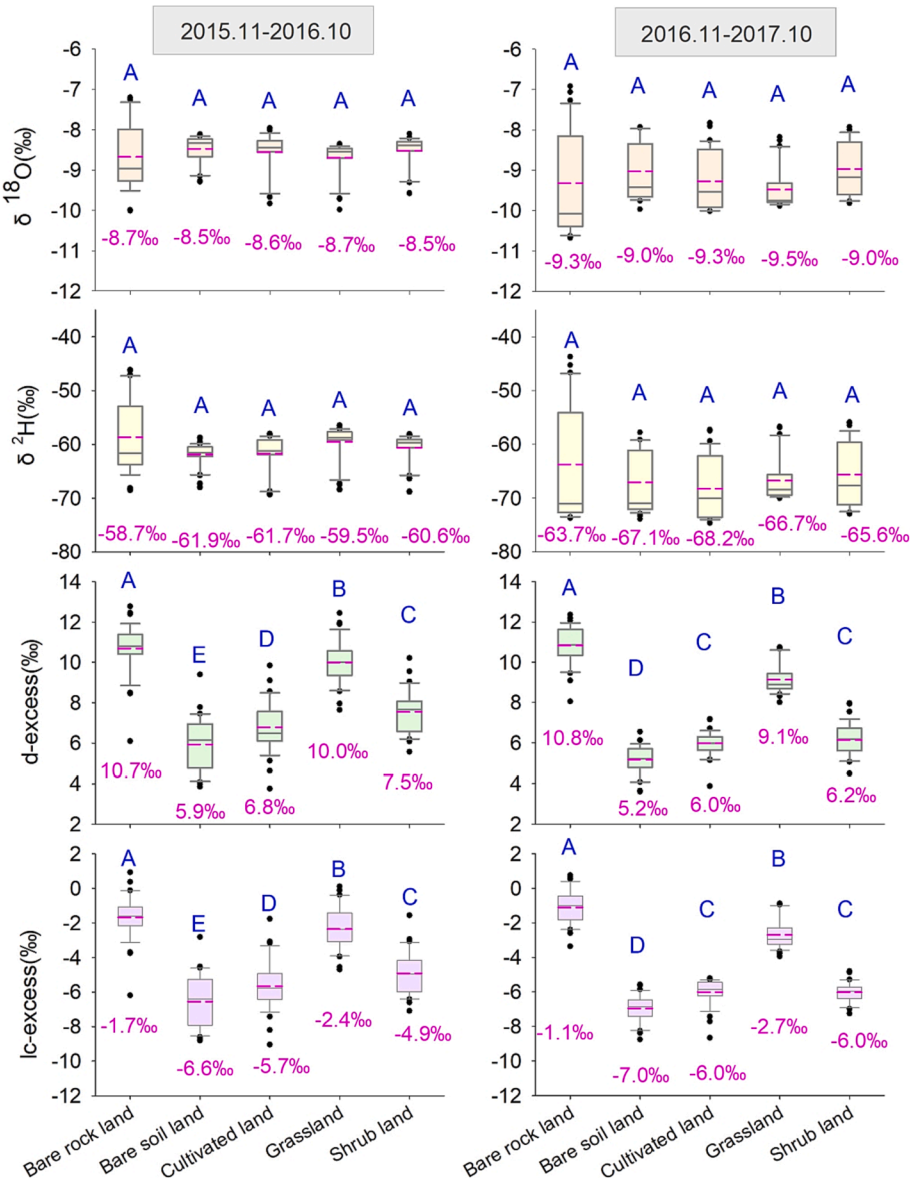

Fig. 7. Box chart of $\delta^{18}O$, $\delta^{2}H$, d-excess, and lc-excess in groundwater. Rose-red dashed line represents annual mean value. A–E, results of multiple comparisons of ANOVA for five land uses. Means start from the highest value. Letters denote significant differences in means ($p < 0.05$).

order: bare-rock land > grassland > shrub land > cultivated land > bare-soil land.

5. Discussion

5.1. Recharge and E of groundwater in simulated watersheds

Fig. 4b1 and b2 shows that the groundwater in the simulated watersheds plotted below the LMWL and had a similar trend with it in $\delta^{18}O$–$\delta^{2}H$ plots. We conclude that the groundwater in the simulated watersheds was recharged by precipitation and suffered from E. The groundwater associated with different land uses deviated from the LMWL to different degrees, with increased deviation indicating more E (Fig. 1). According to Fig. 4b1 and b2, it can be inferred that the integrated degrees of deviation for bare-rock land and grassland were the lowest, followed by those for shrub and cultivated, and bare-soil lands. Thus, the degree of E was the highest for bare-soil land, followed by those for cultivated and shrub lands, and then grassland and bare-rock land.

We found that the degree of E could not be simply expressed by the slope of groundwater in $\delta^{18}O$–$\delta^{2}H$ plots, since a lower slope than the LMWL is generally used to identify whether a water body undergoes E (Wan and Liu 2016, Wang et al. 2019). The slopes of groundwater in the five simulated watersheds were lower than that of LMWL between November 2015 and October 2016 (Fig. 4b1). In contrast, there existed groundwaters between November 2016 and October 2017 almost equal to or exceeded that of LMWL, e.g., shrub land (Fig. 4b2). Others have found similar phenomena (Yang et al. 2015; Dai et al., 2020). In fact, the slope of groundwater is determined by the degrees of E that affected replenishing precipitation events. For example, when precipitation events A and A' undergo various degrees of E to become groundwater B and B' (Fig. 8a), C and C' (Fig. 8b), or C and B' (Fig. 8c), groundwater slopes could become smaller, higher, or equal to that of the GMWL or the LMWL (Fig. 8). Although the slopes of groundwater were different in Fig. 8a and b, the integrated degrees of groundwater E were the same, given their identical integrated degrees of deviation with respect to GMWL. Thus, as groundwater is recharged by several precipitation events during a hydrological year, the slope of groundwater will be determined by E affecting these events. In comparison, Dai et al., (2020) found that soil water with higher slopes than the LMWL resulted from

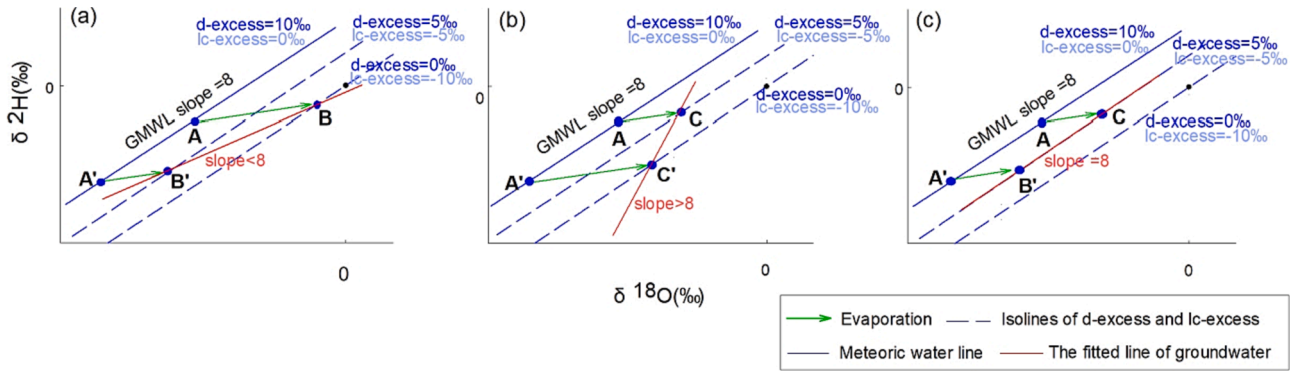

Fig. 8. Slopes of groundwater in $\delta^{18}O$-$\delta^{2}H$ plots resulting from various degrees of evaporation affecting replenishing precipitation events. Values for GMWL and s are identical to those used to develop Fig. 1.

various degrees of E of precipitation in warm and cold seasons. Besides, mixing processes that occur throughout the year also influence the slope. As a result, the slope of groundwater could not be used as a robust indicator of the degree of integrated E.

5.2. *Differences in variations between $\delta^{18}O$, $\delta^{2}H$, d-excess, and lc-excess in rainy season precipitation*

In monsoon regions, precipitation is primarily concentrated in the rainy season, resulting in groundwater being primarily recharged during this time (Table 1). Therefore, the isotopic characteristics of rainy season precipitation are essential to those of groundwater in watersheds. Fig. 5 shows that the d-excess and lc-excess of precipitation during the rainy season exhibited greater stability than $\delta^{18}O$ and $\delta^{2}H$, which notably decreased from May, reached a nadir around mid-August and then increased until October. This was confirmed by the lower STDEVs for d-excess and lc-excess than $\delta^{18}O$ and $\delta^{2}H$ during the rainy seasons of 2016 and 2017 (Table 2).

Fig. 9 shows a schematic map based on the isotopic theory that illustrates variations in $\delta^{18}O$, $\delta^{2}H$, d-excess, and lc-excess during the formation of rainy season precipitation. This map was drawn to determine why d-excess and lc-excess are more stable than $\delta^{18}O$ and $\delta^{2}H$. During the rainy season, water vapor primarily comes from seawater evaporation. According to the evaporation model proposed by Craig and Gordon (1965), seawater evaporation will first form equilibrium vapor (e.g., V_0 and $V_{0.}$) and then atmospheric vapor (e.g., V_1 and $V_{1.}$) (Fig. 9) during the processes by which temperature and humidity affect the values of $\delta^{18}O$, $\delta^{2}H$, d-excess, and lc-excess of the vapor formed as a result of isotopic equilibrium and dynamic fractionation. Furthermore, atmospheric water vapor (e.g., V_1) will condense into precipitation along the meteoric water line (MWL) to various degrees, accompanied by different values of $\delta^{18}O$ and $\delta^{2}H$ but the same d-excess and lc-excess (e.g., A′ and A) (Fig. 9). Given that the water vapor during the rainy season originates primarily from low-latitude oceans, the influence of seawater on rainfall isotopic composition can be negligible (Tracy et al., 1999; Tan, 2014). However, in the process of water vapor transport, the $\delta^{18}O$ and $\delta^{2}H$ values of condensed precipitation will change along the MWL because of rainout to different degrees, whereas d-excess and lc-excess remain relatively unchanged. As a result, d-excess and lc-excess exhibit greater stability than $\delta^{18}O$ and $\delta^{2}H$ during rainy season precipitation.

5.3. *Differences in E indicated by $\delta^{18}O$, $\delta^{2}H$, d-excess, and lc-excess*

We investigated differences in E among the five watersheds based on the annual mean values of $\delta^{18}O$, $\delta^{2}H$, d-excess, and lc-excess in their groundwaters from November 2015 to October 2017. Figs. 6 and 7 show seasonal variations in $\delta^{18}O$ and $\delta^{2}H$ values of groundwater in the five watersheds. Their annual mean values did not significantly differ according to land use ($p < 0.05$), and isotopic enrichment of relationships

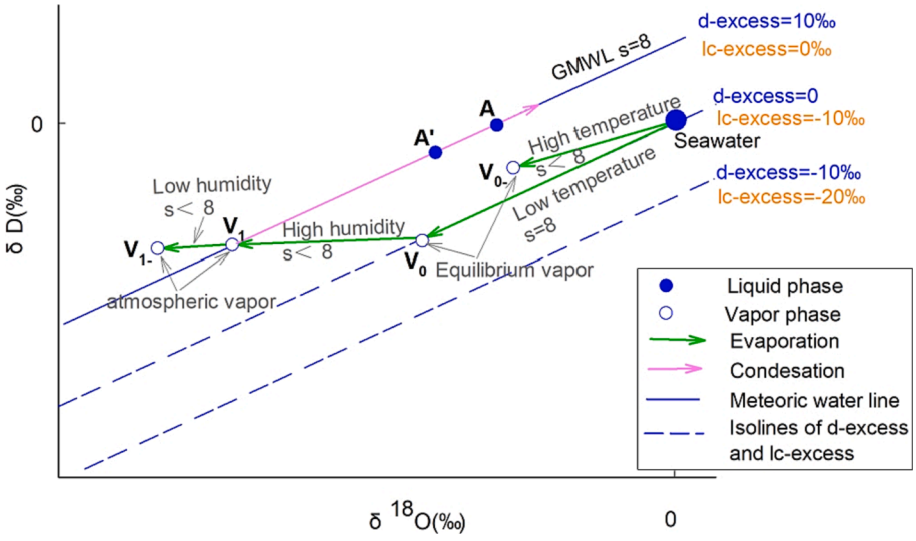

Fig. 9. Schematic illustration of variations in $\delta^{18}O$, $\delta^{2}H$, d-excess, and lc-excess when precipitation formation in rainy season. Values for GMWL and s are identical to those used to develop Fig. 1.

corresponding to degrees of E in $\delta^{18}O$–$\delta^{2}H$ plots were not found (Section 5.1). In other words, $\delta^{18}O$ and $\delta^{2}H$ should be the most enriched in bare-soil land, followed by cultivated and shrub lands, and the most depleted in grassland and bare-rock land. However, this was not observed (Figs. 6 and 7). Furthermore, from November 2015 to October 2016, the annual means of $\delta^{18}O$ and $\delta^{2}H$ in groundwater ($\delta^{18}O = -8.7$ ‰ to -8.5 ‰, $\delta^{2}H = -61.9$ ‰ to -58.7 ‰) were not more enriched than that in precipitation ($\delta^{18}O = -8.3$ ‰, $\delta^{2}H = -54.3$ ‰). Therefore, $\delta^{18}O$ and $\delta^{2}H$ could not reflect E of the five watersheds based on isotopic enrichment between outflowing water (groundwater), and its precipitation input (Ferguson et al., 2007; Jasechko et al., 2013; Good et al., 2015; Gibson et al., 2021). Similar situations were either found by others (Soulsby et al., 2000). In this case, it will cause an underestimation of E and an overestimation of T/ET. However, the seasonal variations of d-excess and lc-excess in groundwater were relatively stable, and their annual means for the land uses during the two years significantly differed ($p < 0.05$; bare-rock land > grassland > shrub land > cultivated land > bare-soil land) and were lower than the annual amount-weighted average of precipitation (Figs. 6 and 7). E intensities was ranked in the following order: bare-soil land > cultivated land > shrub land > grassland > bare-rock land, which was the same in $\delta^{18}O$–$\delta^{2}H$ plots.

This begs the question of why the degree of E indicated by $\delta^{18}O$ and $\delta^{2}H$ differed from those indicated by d-excess and lc-excess. Given that groundwater is primarily recharged by rainy season precipitation, its isotopic characteristics greatly influence those of groundwater. The $\delta^{18}O$ and $\delta^{2}H$ values considerably varied in rainy season precipitation due to the impact of rainout, and groundwater inherited these variations (i.e., evident seasonal variations existed in $\delta^{18}O$ and $\delta^{2}H$ values of groundwater). Consequently, $\delta^{18}O$ and $\delta^{2}H$ signals of groundwater at the outlet of the watershed not only reflected watershed E but were also affected by the changing input of $\delta^{18}O$ and $\delta^{2}H$ via precipitation. This interfered with, or even masked the signal of watershed E, and might explain the higher T/ET estimates determined using isotope-based methods (Schlesinger and Jasechko, 2014; Sutanto et al., 2014). However, d-excess and lc-excess values in rainy season precipitation were more stable than $\delta^{18}O$ and $\delta^{2}H$. For example, A and A′ (Fig. 1) with different $\delta^{18}O$ and $\delta^{2}H$ values but the same d-excess and lc-excess values, when they underwent same degree of E to become B and B′, their d-excess and lc-excess values were the same, despite their $\delta^{18}O$ and $\delta^{2}H$ values being different. As a result, the d-excess and lc-excess groundwater signals were less affected by precipitation input variability and might be more effective as watershed E signals.

We found significant and positive correlations between d-excess and lc-excess in groundwaters of the five watersheds (Fig. 10), which is reasonable because they originated from the $\delta^{18}O$ and $\delta^{2}H$ dual-isotope values and were essentially determined by the linear MWL relationship. Trends in d-excess and lc-excess values increased from bare-soil to cultivated and shrub lands, and to grassland and bare-rock land. Therefore, both values could be considered good isotopic indexes for estimating watershed E.

5.4. Partitioning of watershed evapotranspiration in the five watersheds by d-excess dual isotopes

Given the close link between d-excess and lc-excess, the E rates of the five simulated watersheds were calculated from d-excess dual isotopes using Eq. (7) (Table 3). Because no plants grew in bare-rock and bare-soil lands, their ET values based on water balance (Table 1) were only from E, which allowed us to verify the E results based on the d-excess dual isotopes. Tables 1 and 3 show that the E values obtained from d-excess agree better with those from the water balance in bare-rock land (7.5 ± 3.8 % vs 5.9 ± 3.3 %, 2.7 ± 2.5 % vs 1.9 ± 1.6 %) than bare-soil land (28.1 ± 3.3 % vs 36.2 ± 2.4 %, 25.3 ± 2.6 % vs 29.8 ± 1.1 %) during the two hydrological years. The results estimated from d-excess are generally lower than those from water balance in bare-soil land. This is because soil cover weakens precipitation infiltration, and some precipitation events retained in soil are almost totally evaporated before they could recharge to groundwater. This leads to the E signal being underestimated by the isotope-based method when those kinds of precipitation fail to circulate to groundwater (Schlaepfer et al., 2014). However, considering the estimated uncertainties existed in the water balance, the watershed E results estimated using the d-excess dual isotopes were dependable.

Based on ET values from the water balance (Table 1) and E values obtained using d-excess (Table 3), values for T in watersheds with developed vegetation were determined (Fig. 11). Fig. 11 shows that infiltration rates decreased in the order of bare-rock without soil or vegetation cover, bare-soil with soil but without vegetation, cultivated, shrub, and grassland with soil cover and increased degrees of vegetation. The infiltration rate decreased from 94.1 % (bare-rock land) to 63.8 % (bare-soil land) to 35.9 % (grassland) and from 98.1 % (bare-rock land) to 70.2 % (bare-soil land) to 35.2 % (grassland) in the two studied years. These findings indicated the important role of soil (30.3 % and 27.9 % reductions) and vegetation (27.9 % and 35.0 % reductions) cover in weakening rainfall infiltration. That is, increased soil and vegetation cover will result in a low infiltration rate, namely a high ET (=1 − infiltration rate). Furthermore, E decreased in the four land uses with soil cover, during the first and second years from 36.2 % to 10.7 % and 29.8 % to 9.9 %, respectively, and T increased from 16.0 % to 52.5 % and 17.0 % to 54.8 %, respectively, with increasing vegetation (Fig. 11). This showed the importance of vegetation cover in controlling E and T. This is because more vegetation cover results in less soil being exposed to the air, resulting in less E and more T. Furthermore, if the vegetation cover is well developed (e.g., grassland), T dominates ET (Fig. 11).

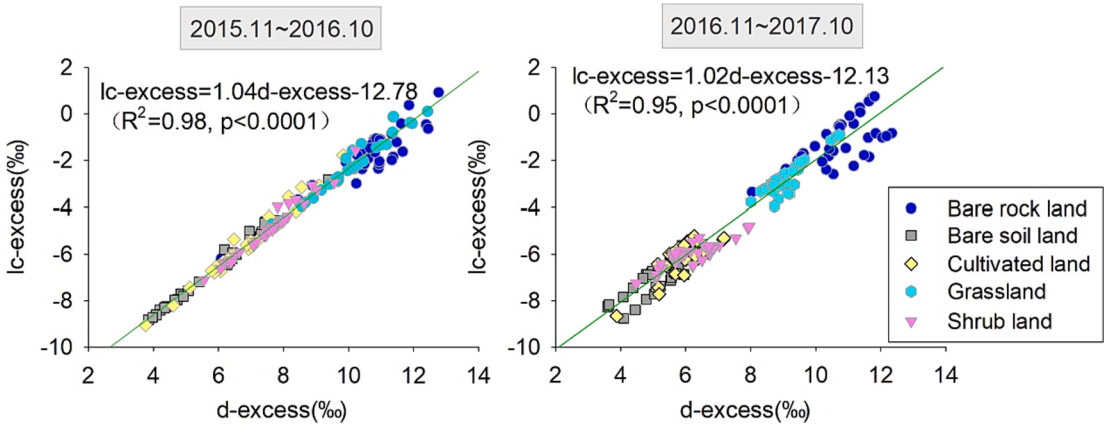

Fig. 10. Plots of d-excess and lc-excess in groundwater from November 2015 to October 2017.

Table 3
Estimated evaporation rate (E) determined using d-excess dual isotopes from November 2015 to October 2017.

Period	Water type	t(°C)[a]	h(%)[a]	$\delta^{18}O_0$[b] (‰)	$\delta^{2}H_0$[b] (‰)	d_0-excess[b] (‰)	$\delta^{18}O$[c] (‰)	$\delta^{2}H$[c] (‰)	d-excess[c] (‰)	E[d] (%)
2015/11–2016/10	Bare rock	16.3	81.6	−8.3	−54.3	12.2	−8.7	−58.7	10.7	7.5 ± 3.8
	Bare soil						−8.5	−61.9	5.9	28.1 ± 3.3
	Cultivated						−8.6	−61.7	6.8	24.4 ± 3.3
	Grassland						−8.7	−59.5	10.0	10.7 ± 4.3
	Shrubland						−8.5	−60.6	7.5	21.6 ± 3.3
2016/11–2017/10	Bare rock	16.8	81.1	−10.4	−72.0	11.4	−9.3	−63.7	10.8	2.7 ± 2.5
	Bare soil						−9.0	−67.1	5.2	25.3 ± 2.6
	Cultivated						−9.3	−68.2	6.0	22.4 ± 2.3
	Grassland						−9.5	−66.7	9.1	9.9 ± 2.6
	Shrubland						−9.0	−65.6	6.2	21.7 ± 2.2

[a] t and h are the annual mean temperature and relative humidity respectively;
[b] $\delta^{18}O_0$, $\delta^{2}H_0$ and d_0-excess are initial isotopic compositions of groundwater inferred from annual amount-weighted mean of precipitation.
[c] $\delta^{18}O$, $\delta^{2}H$ and d-excess are annual mean isotopic compositions of groundwater at watershed outlet.
[d] E represents evaporation rate, estimated by E = 1-f, where f is residual fraction of initial water and calculated from Eq. (7).

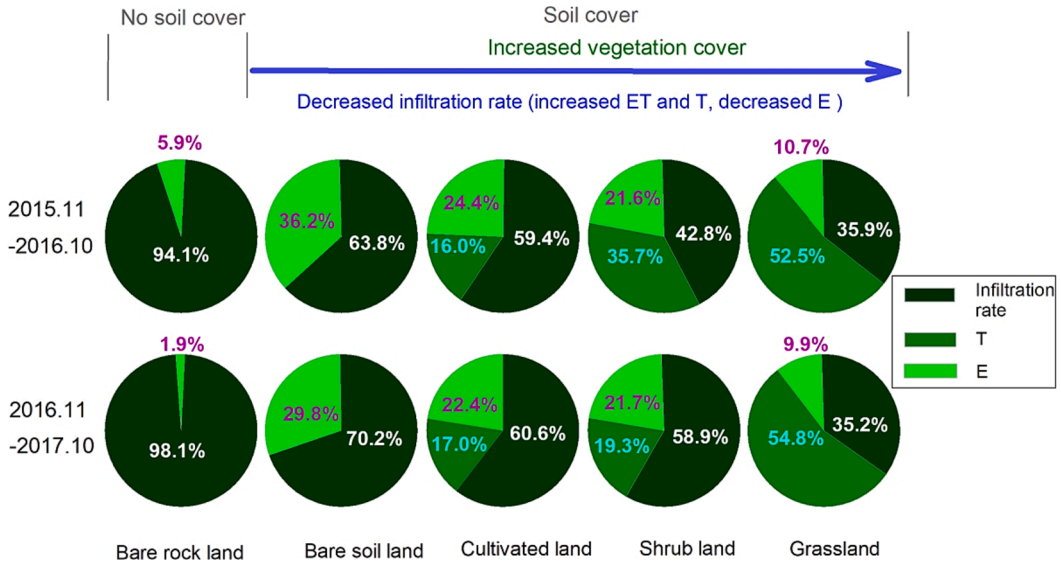

Fig. 11. Partitioning of watershed water components under different land uses into infiltration rate, evaporation (E), and transpiration (T) from November 2015 to October 2017.

6. Conclusions

We aimed to determine differences in the ability of hydrogen and oxygen single isotopes and their dual isotopes to indicate watershed evaporation. We therefore simulated five watersheds with different land uses at the Shawan Test Site, Southwest China, which has a subtropical monsoon climate. We found that d-excess and lc-excess dual isotopes were better indicators of watershed evaporation than $\delta^{18}O$ and $\delta^{2}H$ single isotopes. This is because $\delta^{18}O$ and $\delta^{2}H$ of precipitation are easily impacted by rainout during the rainy season, when groundwater is primarily recharged, and are more variable than d-excess and lc-excess. This leads to $\delta^{18}O$ and $\delta^{2}H$ in groundwater being more vulnerable to changing isotopic signal input in precipitation. In turn, this can interfere with, or mask the watershed evaporation signal carried by $\delta^{18}O$ and $\delta^{2}H$. Evaporation estimated using d-excess dual isotopes closely agreed with estimates obtained based on water balance in bare-rock and bare-soil lands without plants. Whereas the low consistency in bare-soil compared with bar-rock reminds us that more attentions need to pay to the effective recharge of precipitation events to groundwater when estimate watershed evaporation based on isotopes in future work. The present findings can help to select suitable isotopic indexes for estimating watershed evaporation, especially in Asian monsoon regions.

CRediT authorship contribution statement

Yundi Hu: Conceptualization, Methodology, Writing – original draft, Software, Data curation, Writing – review & editing. **Hongdai Fan:** Software, Visualization, Formal analysis. **Min Zhao:** Data curation, Investigation, Writing – review & editing. **Deyong Hu:** Data curation, Investigation, Software. **Qian Bao:** . **Cheng Zeng:** Conceptualization, Investigation. **Dong Li:** Data curation, Software. **Yi Zhang:** Data curation, Investigation. **Fan Xia:** Data curation, Investigation. **Xianli Cai:** Data curation, Investigation. **Jia Chen:** Data curation. **Zhongfa Zhou:** Supervision, Writing – review & editing.

Declaration of Competing Interest

The authors declare that they have no known competing financial interests or personal relationships that could have appeared to influence the work reported in this paper.

Data availability

Data will be made available on request.

Acknowledgements

This work was supported by the National Natural Science Foundation of China (42072278, 42177248, 42161048 and 41807366), the Guizhou Science and Technology Supporting Plan (No. 2020-4Y013) and funding from Guizhou Normal University ([2021]26).

References

Bao, Q., Liu, Z., Zhao, M., Hu, Y., Li, D., Han, C., Wei, Y., Ma, S., Zhang, Y., 2020. Primary productivity and seasonal dynamics of planktonic algae species composition in karst surface waters under different land uses. J. Hydrol. 591, 125295.

Beer, C., Reichstein, M., Ciais, P., Farquhar, G.D., Papale, D., 2007. Mean annual GPP of Europe derived from its water balance. Geophys. Res. Lett. 34, L05401.

Berg, A., Sheffield, J., 2019. Evapotranspiration partitioning in CMIP5 models: uncertainties and future projections. J. Climate 32, 2653–2671.

Clark, I.D., Fritz, P., 1997. Environmental Isotopes in Hydrogeology. Lewis, Boca Ration.

Craig, H., 1961. Isotopic variations in meteoric waters. Science 133, 1702–1703.

Craig, H., Gordon, L.I., 1965. Deuterium and oxygen-18 variations in the ocean and the marine atmosphere. In: Tongiorgi E (Ed.), Stable Isotope in Oceanographic Studies and Paleotemperatures, pp. 9–122.

Dai, J., Zhang, X., Luo, Z., Wang, R., Liu, Z., He, X., Rao, Z., Guan, H., 2020. Variation of the stable isotopes of water in the soil-plant-atmosphere continuum of a Cinnamomum camphora woodland in the East Asian monsoon region. J. Hydrol. 589, 125199.

Dansgaard, W., 1964. Stable isotopes in precipitation. Tellus 16 (4), 436–468.

Ehleringer, J.R., Dawson, T.E., 1992. Water uptake by plants: perspectives from stable isotope composition. Plant Cell Environ. 15 (9), 1073–1082.

Evaristo, J., Jasechko, S., McDonnell, J.J., 2015. Global separation of plant transpiration from groundwater and streamflow. Nature 525, 91–94.

Ferguson, P.R., Veizer, J., 2007. Coupling of water and carbon fluxes via the terrestrial biosphere and its significance to the Earth's climate system. J. Geophys. Res. 112, D24S06.

Ferguson, P.R., Weinrauch, N., Wassenaar, L.I., Mayer, B., Veizer, J., 2007. Isotopic constraints on water, carbon, and heat fluxes from the northern Great Plains region of North America. Glob. Biogeochem. Cycles 21, GB2023.

Gibson, J.J., Edwards, T.W.D., Bursey, G.G., 1993. Estimating evaporation using stable isotopes: quantitative results and sensitivity analysis for two catchments in Northern Canada. Nordic Hydrol. 24, 79–94.

Gibson, J.J., Holmes, T., Stadnyk, T.A., Birks, S.J., Eby, P., Pietroniro, A., 2021. Isotopic constraints on water balance and evapotranspiration partitioning in gauged watersheds across Canada. J. Hydrol.-Reg. Stud. 37, 100878.

Gonfiantini, R., Wassenaar, L.I., Araguas-Araguas, L., Aggarwal, P.K., 2018. A unified Craig-Gordon isotope model of stable hydrogen and oxygen isotope fractionation during fresh or saltwater evaporation. Geochim. Cosmochim. Acta 235, 224–236.

Gonfiantini, R., 1986. Environmental isotopes in lake studies. In Handbook of Environmental Isotope Geochemistry (eds. P. Fritz and J. C. Fontes). pp. 113–168.

Good, S.P., Noone, D., Bowen, G., 2015. Hydrologic connectivity constrains partitioning of global terrestrial water fluxes. Science 349 (6244), 175–177.

Han, J., Tian, L., Cai, Z., Ren, W., Liu, W., Li, J., Tai, J., 2022. Season-specific evapotranspiration partitioning using dual water isotopes in a Pinus yunnanensis ecosystem, southwest China. J. Hydrol. 608, 127672.

Horita, J., Rozanski, K., Cohen, S., 2008. Isotope effects in the evaporation of water: a status report of the Craig-Gordon model. Isot. Environ. Healt. Stud. 44 (1), 23–49.

Hu, Y., Liu, Z., Zhao, M., Zeng, Q., Zeng, C., Chen, B., Chen, C., He, H., Cai, X., Chen, J., 2018. Using deuterium excess, precipitation and runoff data to determine evaporation and transpiration: a case study from the Shawan Test Site, Puding, Guizhou. China. Geochim. Cosmochim. Acta 242, 21–33.

Hu, Y., Liu, Z., Ford, D., Zhao, M., Bao, Q., Zeng, C., Gong, X., Wei, Y., Cai, X., Chen, J., 2020. Conservation of oxygen and hydrogen seasonal isotopic signals in meteoric precipitation in groundwater: An experimental tank study of the effects of land cover in a summer monsoon climate. Geochim. Cosmochim. Acta 284, 254–272.

Huang, T., Pang, Z., 2012. The role of deuterium excess in determining the water salinisation mechanism: a case study of the arid Tarim River Basin, NW China. Appl. Geochem. 27 (12), 2382–2388.

Jasechko, S., Sharp, Z.D., Gibson, J.J., Birks, S.J., Yi, Y., Fawcett, P.J., 2013. Terrestrial water fluxes dominated by transpiration. Nature 496, 347–350.

Kool, D., Agam, N., Lazarovitch, N., Heitman, J.L., Sauer, T.J., Ben-Gal, A., 2014. A review of approaches for evapotranspiration partitioning. Agric. Forest Meteorol. 184, 56–70.

Landwehr, J.M., Coplen, T.B., 2004. Line-conditioned excess: a new method for characterizing stable hydrogen and oxygen isotope ratios in hydrologic systems. International conference on isotopes in environmental studies. IAEA Vienna, 132–135.

Lee, D., Veizer, J., 2003. Water and carbon cycles in the Mississippi River basin: potential implications for the Northern Hemisphere residual terrestrial sink. Glob. Biogeochem. Cycles 17 (2), 1–17.

Lis, G., Wassenaar, L.I., Hendry, M.J., 2008. High-precision laser spectroscopy D/H and $^{18}O/^{16}O$ measurements of microliter natural water samples. Anal. Chem. 80 (1), 287–293.

Lyu, S., Wang, J., Song, X., Wen, X., 2021. The relationship of δD and $\delta^{18}O$ in surface soil water and its implications for soil evaporation along grass transects of Tibet, Loess, and Inner Mongolia Plateau. J. Hydrol. 600, 126533.

Majoube, M., 1971. Fractionation of oxygen-18 and deuterium in water vapor. J. Chem. Phys. 68, 1423–1436.

Mitchell, P.J., Veneklaas, E., Lambers, H., Burgess, S.S., 2009. Partitioning of evapotranspiration in a semi-arid eucalypt woodland in south-western Australia. Agric. For. Meteorol. 149 (1), 25–37.

Ren, X., Jia, J., Chen, Y., Hu, Y., Wang, Y., Wu, R., Hu, L., 2022. Comparison of two isotope-based methods used in determining forest evapotranspiration partitioning. Ecol. Ind. 139, 108937.

Schlaepfer, D.R., Ewers, B.E., Shuman, B.N., Williams, D.G., Frank, J.M., Massman, W.J., Lauenroth, W.K., 2014. Terrestrial water fluxes dominated by transpiration: comment. Ecosphere 5 (5), art 61.

Schlesinger, W.H., Jasechko, S., 2014. Transpiration in the global water cycle. Agric. For. Meteorol. 180–190, 115–117.

Soulsby, C., Malcolm, R., Helliwell, R., Ferrier, R.C., Jenkins, A., 2000. Isotope hydrology of the Allt a' Mharcaidh catchment, Cairngorms, Scotland: implications for hydrological pathways and residence times. Hydrol. Process. 14, 747–762.

Sulman, B.N., Roman, D.T., Scanlon, T.M., Wang, L.X., Novick, K.A., 2016. Comparing methods for partitioning a decade of carbon dioxide and water vapor fluxes in a temperate forest. Agric. For. Meteorol. 226, 229–245.

Sutanto, S.J., Van den Hurk, B., Dirmeyer, P.A., Seneviratne, S.I., Rockmann, T., Trenberth, K., Blyth, E.M., Wenninger, J., Hoffmann, G., 2014. HESS Opinions "A perspective on isotope versus non-isotope approaches to determine the contribution of transpiration to total evaporation". Hydrol. Earth. Syst. Sci. 18 (8), 2815–2827.

Tan, M., 2014. Circulation effect: response of precipitation $\delta^{18}O$ to the ENSO cycle in monsoon regions of China. Clim. Dyn. 42, 1067–1077.

Telmer, K., Veizer, J., 2000. Isotopic constraints on the transpiration, evaporation, energy, and gross primary production Budgets of a large boreal watershed: Ottawa River Basin, Canada. Glob. Biogeochem. Cycles 14 (1), 149–165.

Tracy, A.M., David, W.L., Howard, J.S., 1999. Glacial–interglacial changes in subantarctic sea surface temperature and $\delta^{18}O$-water using foraminiferal Mg. Earth Planet. Sci. Lett. 170 (4), 417–432.

Van der Tol, C., Gash, J.H.C., Grant, S.J., McNeil, D.D., Robinson, M., 2003. Average wet canopy evaporation for a Sitka spruce forest derived using the eddy correlation energy balance technique. J. Hydrol. 276, 12–19.

Wan, H., Liu, W.G., 2016. An isotope study ($\delta^{18}O$ and δD) of water movements on the Loess Plateau of China in arid and semiarid climates. Ecol. Eng. 93, 226–233.

Wang, J., Lu, N., Fu, B.J., 2019. Inter-comparison of stable isotope mixing models for determining plant water source partitioning. Sci. Total Environ. 666, 685–693.

Wang, X.F., Yakir, D., 2000. Using stable isotopes of water in evapotranspiration studies. Hydrol. Process. 14, 1407–1421.

Wershaw, R.L., Friedman, I., Heller, S.J., Frank, P.A., 1966. Hydrogen isotopic fractionation of water passing through trees. In: Hobson G D and Speers G C (Ed.), Advanced in Organic Geochemistry, pp.55–67.

Williams, D.G., Cable, W., Hultine, K., Hoedjes, J.C.B., Yepez, E.A., Simonneaux, V., Er-Raki, S., Boulet, G., de Bruin, H.A.R., Chehbouni, A., Hartogensis, O.K., Timouk, F., 2004. Evapotranspiration components determined by stable isotope, sap flow and eddy covariance techniques. Agr. Forest Meteorol. 125, 241–258.

Wisler, C.O., Brater, E.F., 1959. Hydrology. John Wiley, New York.

Xiao, W., Wei, Z., Wen, X., 2018. Evapotranspiration partitioning at the ecosystem scale using the stable isotope method—A review. Agric. For. Meteorol. 263, 346–361.

Yang, R., Liu, Z., Zeng, C., Zhao, M., 2012. Response of epikarst hydrochemical changes to soil CO_2 and weather conditions at Chenqi, Puding, SW China. J. Hydrol. 468, 151–158.

Yang, B., Wen, X., Sun, X.M., 2015. Seasonal variations in depth of water uptake for a subtropical coniferous plantation subjected to drought in an East Asian monsoon region. Agric. For. Meteorol. 201, 218–228.

Yepez, E.A., Williams, D.G., Scott, R.L., Lin, G., 2003. Partitioning overstory and understory evapotranspiration in a semiarid savanna woodland from the isotopic composition of water vapor. Agric. For. Meteorol. 119, 53–68.

Zeng, Q., Liu, Z., Chen, B., Hu, Y., Zeng, S., Zeng, C., Yang, R., He, H., Zhu, H., Cai, X., Chen, J., Ou, Y., 2017. Carbonate weathering-related carbon sink fluxes under different land uses: a case study from the Shawan Simulation Test Site, Puding, Southwest China. Chem. Geol. 474, 58–71.

Zhao, M., Zeng, C., Liu, Z., Wang, S., 2010. Effect of different land use/land cover on karst hydrogeochemistry: a paired catchment study of Chenqi and Dengzhanhe, Puding, Guizhou, SW China. J. Hydrol. 388, 121–130.

Zhao, M., Hu, Y., Zeng, C., Liu, Z., Yang, R., Chen, B., 2018. Effects of land cover on variations in stable hydrogen and oxygen isotopes in karst groundwater: a comparative study ofthree karst catchments in Guizhou Province, Southwest China. J. Hydrol. 565, 374–385.

Zhou, H., Zhang, X., Yao, T., Hua, M., Wang, X., Rao, Z., He, X., 2019. Variation of $\delta^{18}O$ in precipitation and its response to upstream atmospheric convection and rainout: a case study of Changsha station, south-central China. Sci. Total Environ. 659, 1199–1208.

Zhu, H., Zeng, C., Liu, Z., Zeng, Q., Li, L., 2015. Karst-related carbon sink flux variations caused by land use changes: an example from the Puding karst test site in Guizhou. Hydrogeol. Engineer. Geol. 42, 120–125 in Chinese with English abstract.